

Characterization of mechanical properties of battery electrode films from acoustic resonance measurements

Kathryn L. Dallon,¹ Jing Yao,¹ Dean R. Wheeler,² and Brian A. Mazzeo^{1,a)}

¹Department of Electrical and Computer Engineering, Brigham Young University, Provo, Utah 84602, USA

²Department of Chemical Engineering, Brigham Young University, Provo, Utah 84602, USA

(Received 8 January 2018; accepted 17 March 2018; published online 2 April 2018)

Measurements of the mechanical properties of lithium-ion battery electrode films can be used to quantify and improve manufacturing processes and to predict the mechanical and electrochemical performance of the battery. This paper demonstrates the use of acoustic resonances to distinguish among commercial-grade battery films with different active electrode materials, thicknesses, and densities. Resonances are excited in a clamped circular area of the film using a pulsed infrared laser, and responses are measured using an electret condenser microphone. A numerical model is used to quantify the sensitivity of resonances to changes in mechanical properties. When the numerical model is compared to simple analytical models for thin plates and membranes, the battery films measured here trend more similarly to the membrane model. Resonance measurements are also used to monitor the drying process. Results from a scanning laser Doppler vibrometer verify the modes excited in the films, and a combination of experimental and simulated results is used to estimate the Young's modulus of the battery electrode coating layer. Published by AIP Publishing. <https://doi.org/10.1063/1.5021809>

I. INTRODUCTION

Due to their large energy density and ability to charge and discharge at high power, lithium-ion (Li-ion) batteries are ideal for many applications. One important area of research to improve these batteries is to understand and measure heterogeneity in battery electrode properties,^{1,2} particularly before the electrode is incorporated into a full cell.

This research investigates the use of acoustic measurements as an alternative means of non-destructive measurement that could be adapted for quality control in battery film manufacturing. Specifically, we report our results in distinguishing among films with different mechanical properties using acoustic resonances. This research has been developed with the long-term goal of an acoustic probe to detect small changes in the film's local material properties, in particular, density and thickness. The proposed acoustic probe would be used in conjunction with a conductivity probe³ to provide better understanding of the electrode properties. This could then inform modeling work as well as process improvements.

The single-sided Li-ion battery electrode films we use are essentially two-layer structures. The metal current collector, generally made of aluminum for cathodes and copper for anodes, is one layer. On top of this layer is a coating layer consisting of the cathode or anode material. In cathodes, this material is a mixture of large active material particles, carbon additive for increased conductivity, polymeric binder, and pores (both large pores and nanopores). This layered structure and its constituent materials are shown in Fig. 1. In this paper, the top layer will be called the coating, while "film" refers to the entire two-layer structure of the electrode.

The homogeneity of the coating layer in battery films is important, in properties such as the thickness and material distribution. Variations in the battery coating properties can create "hot" and "cold" areas of conductivity across the electrode, which can lead to increasing defects over time as the battery is used. Measuring the mechanical properties of lithium-ion battery films, such as the thickness and elasticity, could be important for predicting and improving homogeneity of the films and subsequent performance of the battery,¹

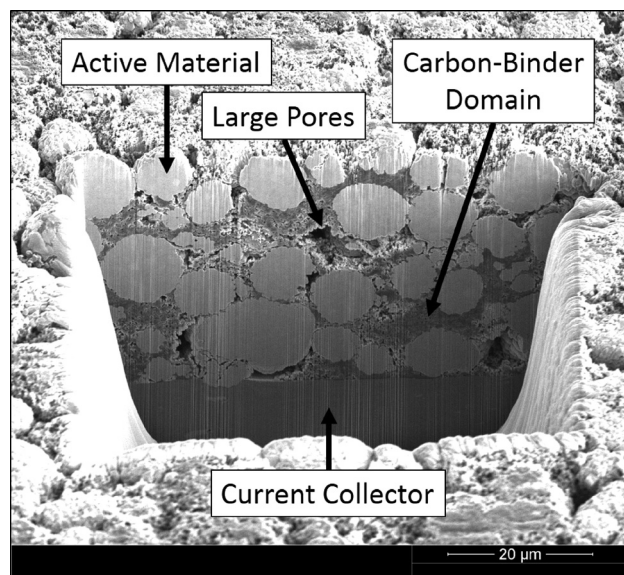


FIG. 1. Scanning electron microscope micrograph of a Li-ion cathode battery film in cross-section, cut using a focused ion beam. The bottom layer is the aluminum current collector. The top layer is the coating and is made up of an active material (lighter circles), carbon conductivity additive and polymeric binder (nanoporous gray filler between the active material and binder), and empty pores (dark spaces between the active material and binder).

^{a)}Electronic mail: bmazzeo@byu.edu

as pristine commercial battery electrodes can exhibit significant variation in structure across a millimeter scale.³ Variations in macroscopic properties, like the thickness, elastic modulus, and tortuosity, can indicate differences in microscopic properties, like material distribution, that cause inhomogeneities in electrical and ionic conductivity.^{2,4}

It would be advantageous if problems with film heterogeneity could be identified and addressed through accurate, non-destructive inspection of the electrode as it is being manufactured. There are several techniques currently used to measure the mechanical characteristics of films, including nanoindentation^{4,5} and Brillouin scattering.^{6,7} However, they have not been extensively used for analyzing battery electrodes.

Acoustics have been used to determine characteristics of thin films using surface acoustic waves^{8–16} and Lamb waves^{17–20} and have even been used to correlate with the state of charge and health in packaged battery cells.²¹ The frequency of vibration of materials has been used in the past to find properties like Young's modulus.^{19,22–25} We extend the use of these acoustic principles to examine battery electrode films.

II. THEORY

A. Resonances

When looking at how films and other thin structures vibrate, the natural frequencies are the frequencies corresponding to the solutions of the two-dimensional wave equation.²⁶ The solutions will change based on the given boundary conditions of the system and are the frequencies at which the system will freely vibrate. If the vibration is forced, resonance occurs when the frequency of the driven force matches the natural frequency of the system.²⁷ These resonance frequencies are those for which the maximum vibration amplitude occurs for a given excitation.²⁶ The resonance frequency of a vibrating object depends on several factors, including the shape, size, and material properties.

When solving for how materials vibrate, thin plates and membranes have similar theory, but membrane theory is somewhat simplified. The only restoring force on a membrane comes from the tension, while a thin plate has a restoring force from its stiffness.²⁶ These two types of systems can be distinguished by the ratio a/h , where a is the characteristic length of the material and h is the thickness. Thin plates typically have an a/h ratio ranging from about 8 to 80, while ratios of $a/h > 80$ are associated with membranes.²⁸ In our case, we are generally looking at a characteristic dimension of $a \approx 1$ cm. The thickness of many battery electrode films ranges from about 20–60 μm , resulting in an a/h ratio ranging from ~ 150 to 500. However, even though the a/h ratio indicates that our films are in the membrane region, they do not fully qualify as membranes, because a true membrane does not have any stiffness. They also do not act fully like a thin plate, due to the ability to put them under significant tension. However, if the tension applied to a film is large enough, the membrane properties dominate and we can approximate it as a membrane with some perturbations due to the rigidity.²⁹ Although our battery films are not fully

described by either thin plate or membrane theory, particularly because these simple theories are for a single layer made of one material and the battery films have two layers, it can be useful to look at the resonance equations for both theories to give us some intuition as to how we can expect the films to behave.

B. Thin plate vs. membrane theory

The fundamental frequency of a circular thin plate with a clamped boundary is given by

$$f_{01} = \frac{\alpha_{01}}{2\pi a^2} \sqrt{\frac{D}{\rho h}}, \quad (1)$$

where $\alpha_{01} = 10.21$, a is the radius of the plate, ρ is the density, h is the thickness, and

$$D = \frac{Eh^3}{12(1-\nu^2)} \quad (2)$$

is the flexural rigidity, with E as the Young's modulus and ν as the Poisson's ratio. The value of α_{ns} changes based on the number of radial and circular nodes in the mode.²⁷ It is noted that f_{01} will linearly increase with h .

The fundamental frequency of a circular, single-layered membrane is given by

$$f_{01} = \frac{\alpha_{01}}{2\pi a} \sqrt{\frac{T}{\rho h}}, \quad (3)$$

where $\alpha_{01} = 2.405$, a is the radius of the membrane, T is the tension, ρ is the density, and h is the thickness.^{27,30,31} It is noted that f_{01} decreases with increasing h .

Equations (1) and (3) show how the mechanical properties affect the resonance frequencies of a material. Both are dependent on the density and thickness, as well as the radius of the vibrating area. Through the rigidity shown in Eq. (2), we see that the thin plate theory also relies on the Young's modulus of the material.

Although not perfect models for the battery electrodes, these equations give an approximate prediction for how the resonance frequency changes with thickness, stiffness, tension, and density. Notably, a parameter such as the thickness can affect the resonance frequency in opposite ways depending on the true underlying physics which are approximated by these models.

C. Simulations

In order to gain further insight into how we expect the films to resonate, and because simple analytical models are not available for more complicated structures, we created a numerical model using the modal analysis in ANSYS 15.0 (ANSYS, Inc.) simulation software. For all of the simulations, the circumference of the circular geometry (both layers, if applicable) is a fixed edge. An example of the simulation geometry with the meshing visible is shown in Fig. 2.

Using ANSYS, we found the frequencies of the first six mode shapes. Each resonance frequency corresponds to a

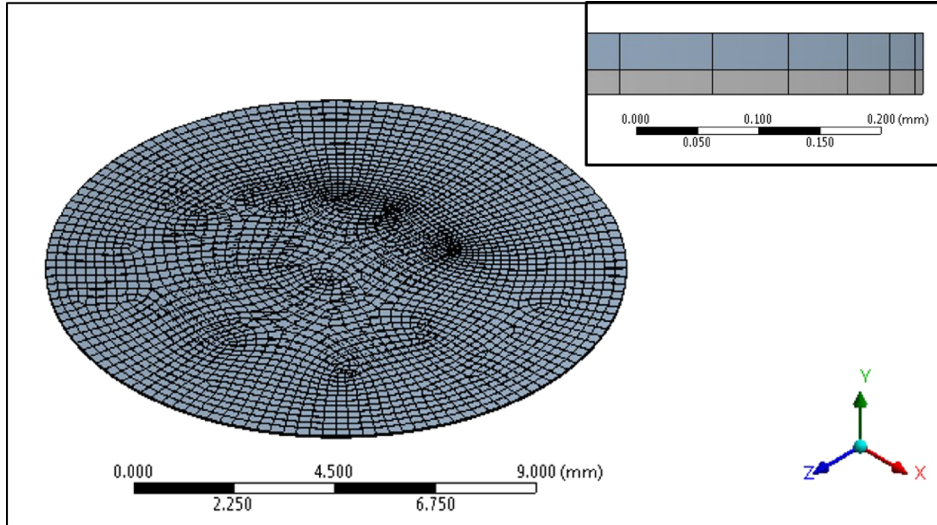


FIG. 2. ANSYS modal analysis simulation, with a radius of 0.65 cm and mesh minimum size of 0.01 mm and maximum size of 0.3 mm. The circumference of the circle is a fixed boundary. The inset shows the side view of the simulation geometry, with the two layers visible.

particular mode shape. Some mode shapes have the same nodal patterns with a different orientation. These degenerate modes occur at the same (in an ideal case) or similar (when anisotropies are present) frequencies. As seen in Fig. 3, for vibration of a circular area with a fixed boundary, this happens with modes 2 and 3 and modes 4 and 5, so we have left the duplicate resonances of modes 3 and 5 out of the subsequent graphs.

The simulation geometry is a disk of radius 0.65 cm with either one layer (aluminum only) or two layers (aluminum current collector and battery coating) with the material properties listed in Table I. The values for the coating properties were taken from a paper by Forouzan *et al.*,³² other than the Poisson's ratio, which was assumed to be the common value²⁶ of 0.3.

In order to better understand the vibration behavior of the battery films, we compare the numerical model given by the simulations to the analytical models given by Eqs. (1) and (3). The numerical model did not involve any pretension on the film, so we do not have an applied tension as required for the membrane model. The tension was reverse-calculated using Eq. (3) and the resonance frequency from the numerical model result for the first mode and the lowest varied parameter value (so the membrane model is identical

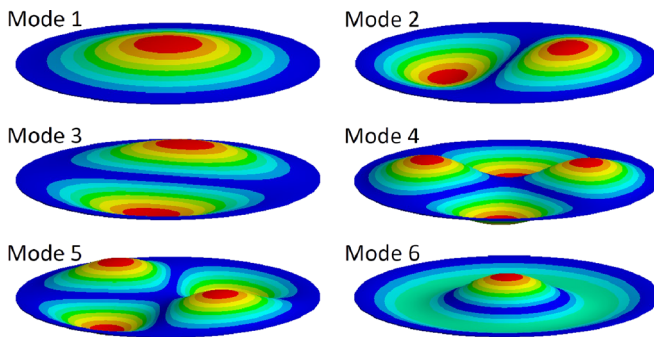


FIG. 3. ANSYS modal analysis simulation, showing the first six mode shapes for a circular area with a fixed boundary. Each mode shape corresponds to a resonance frequency. Modes 2 and 3 and modes 4 and 5 have the same nodal patterns (one and two nodal diameters, respectively) but with different orientations, and they occur at the same or nearly the same frequencies.

to the simulation for the first point of the first mode). Since the analytical models are both for a single-layer structure, composite parameters were calculated for the battery film using the weighted averages in the rule of mixtures.³³ The total thickness, h_t , was calculated using

$$h_t = h_c + h_m, \quad (4)$$

where h_c is the coating thickness and h_m is the current collector (metal) thickness. The composite density, ρ_t , was calculated using the rule of mixtures

$$\rho_t = \frac{\rho_c h_c + \rho_m h_m}{h_t}, \quad (5)$$

where ρ_c and ρ_m are the densities of the coating and current collector, respectively. Calculating the composite Poisson's ratio is also done using Eq. (5), but using Poisson's ratio ν in place of ρ . The composite Young's modulus, E_t , was also calculated using the rule of mixtures, but this takes an inverse form for elasticity.

$$E_t^{-1} = \frac{E_c^{-1} h_c + E_m^{-1} h_m}{h_t}, \quad (6)$$

where E_c and E_m are the Young's moduli of the coating and current collector. This equation gives the series, or transverse, effective Young's modulus, which is only an estimation, as the motion of the film is not strictly confined to one direction, but it is essentially a lower limit on the composite value. Using an equation with the same form as Eq. (5) would give the parallel, or longitudinal, effective modulus, which is the upper limit.³³

Simulations of aluminum foil (without any battery coating) have more characteristics of a thin plate; in particular,

TABLE I. Material parameters used in the numerical and analytical models.

Material	h (μm)	ρ (g/cm^3)	E (GPa)	ν
Aluminum	20	2.70	70	0.334
Coating	30	2.029	0.01132	0.3

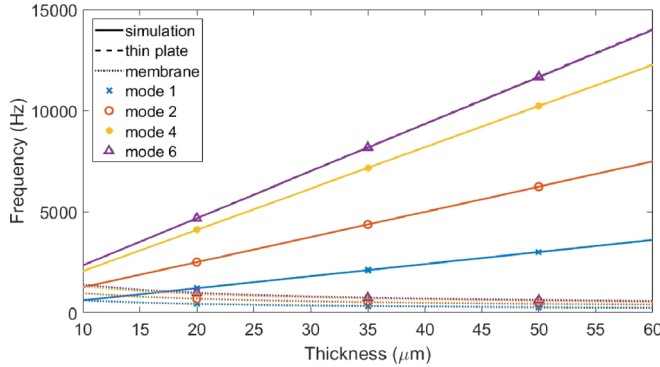


FIG. 4. Numerical and analytical models (for both the thin plate and membrane) of a circular aluminum film (no battery coating) with a fixed boundary, radius of 0.65 cm, and varying thickness. The first four unique resonance mode shapes are shown. The simulation results (solid line) correspond very closely with and therefore obscure the corresponding thin plate analytical model results.

the resonance frequency increases with thickness through the rigidity. This is seen in Fig. 4, where the simulated modes (shown by the solid line) correspond very well with the thin plate model (shown by the dashed line, which is barely visible under the solid line), but do not follow the trend of the membrane model (shown by the dotted line).

In contrast, the simulations demonstrate that the layered configuration of the battery electrode sometimes acts like a thin plate, but more often like a membrane. For the battery film simulations, with the two-layer structure, one of the battery coating parameters (thickness, density, or Young's modulus) was varied for each set of results, while the others were held constant. These comparisons are given in Figs. 5–7. Unlike the aluminum model, the simulations of battery films show the resonance frequency decreasing with increasing coating thickness, demonstrating more membrane-like behavior. This is illustrated in Fig. 5, where the resonance frequency decreases as the coating thickness increases, and the simulations more closely correspond with the membrane model.

In Fig. 6, the coating thickness is at a constant value of 30 μm and the coating density is varied. As expected from both simplified models in Eqs. (1) and (3), an increase in density corresponds to a decrease in resonance frequency.

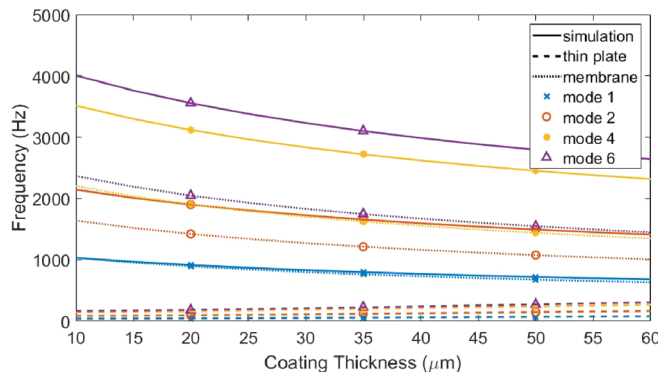


FIG. 5. Numerical and analytical models of circular battery cathode (two layers: coating and aluminum current collector) with a fixed boundary, radius of 0.65 cm, and the material properties listed in Table I. The thickness of the coating was varied to find the resonance frequencies for four mode shapes.

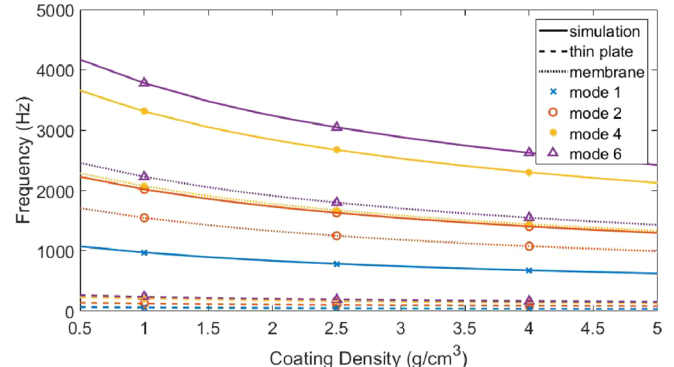


FIG. 6. Numerical and analytical models of circular battery cathode with a radius of 0.65 cm, and the material properties listed in Table I. The density of the coating was varied to find the resonance frequencies for four mode shapes.

The numerical model results still match more closely with the analytical model for membranes.

When simulating different Young's moduli, as shown in Fig. 7, an increase in the Young's modulus of the coating layer causes an increase in resonance frequency. This is expected from the forms of Eqs. (1) and (2). In this case, the simulated results do not match as closely with either thin plate or membrane theory, since the membrane theory does not rely on the Young's modulus.

The numerical and simplified analytical models do not always correlate well, but experiments on real films can validate or refine the theoretical analysis. The combination of experimental results and numerical simulations can also lead to additional information by estimating the unknown parameters of the battery electrodes.

III. EXPERIMENTAL METHODS

A. Resonance measurements

The measurement apparatus consisted of a custom clamp to confine the vibrating area of the film, an excitation source, and a microphone on the opposite side of the clamp. The excitation source was a pulsed infrared laser, as shown in Fig. 8. When orienting the films so that the coating side faced the laser, microscope slides (each 1.2 mm thick) were

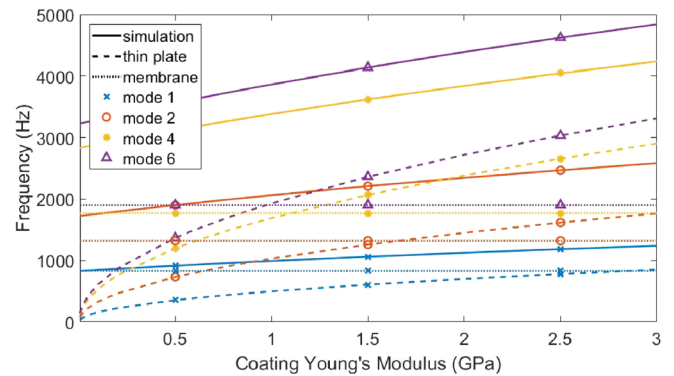


FIG. 7. Numerical and analytical models of the circular battery cathode with a radius of 0.65 cm, and the material properties listed in Table I. The Young's modulus of the coating was varied to find the resonance frequencies for four mode shapes.

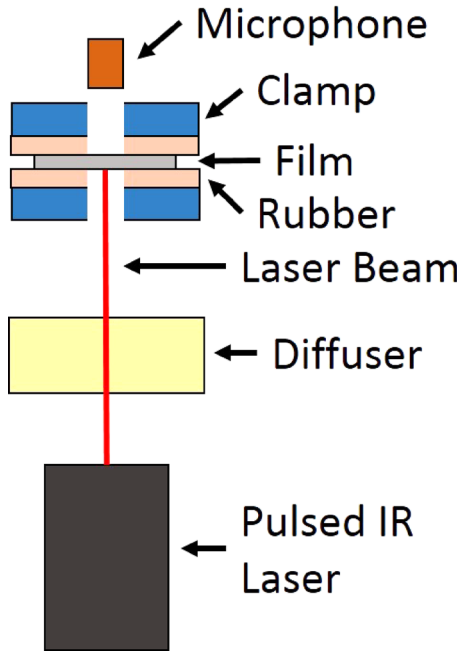


FIG. 8. Illustration of the cross-sectional view of the setup for the resonance measurements using a laser for excitation. The laser beam excites a vibration in the area of the film confined by the clamp, and a microphone behind the clamp records the acoustic response of the film. When the film is oriented with the coating side facing the laser, the beam is attenuated to avoid film ablation.

placed between the laser and the clamped film in order to attenuate the laser sufficiently to avoid ablation of the film coating. A clamp was needed to securely confine the edges of the film to obtain a circular area with a clamped boundary. As seen in Eqs. (1)–(3), different boundary conditions, tension, and area will change the resonance response of the material, so we ensured that these were consistent between experiments. The clamp was made of two steel plates ($7.6\text{ cm} \times 7.65\text{ cm} \times 0.4\text{ cm}$) with a hole (diameter 1.28 cm) drilled through the middle of each for the vibration area. Steel pins (length 2.85 cm , diameter 0.4 cm) were fixed into the corners of the bottom plate, and the corresponding holes (diameter 0.5 cm) were drilled in each of the four corners of the top plate for alignment. Rubber sheets (1.25 mm thick, durometer Shore 19A) were placed in between the steel plates to make sure full contact was made with the film and weights (1253.6 g) were placed on top to provide full clamping of the circumference of the vibration area.

B. Laser

The pulsed laser beam excites the film by briefly heating it up.^{17,18} This in turn creates a vibration in the material. We used a pulsed infrared laser from Standa (model STA-01-8-1053). This laser has a wavelength of 1053 nm and can be turned on via an external trigger for short bursts (about 500 ps in length). The reflectivity of the material at the wavelength of the laser can also be problematic. Aluminum reflects infrared light very well (smooth aluminum has over 90% reflectivity, and rough aluminum can have over 50% reflectivity³⁴) so it does not absorb much of the laser energy. When testing our setup with aluminum foil, which is very

similar to the current collector layer on our films, often insufficient energy was being absorbed to excite a large vibration. When we switched to battery films (with a coating which, unlike aluminum, is dark and not shiny), we found that too much energy was being absorbed and the film was being damaged. Thus, different materials require different levels of attenuation for the laser in order to avoid damage, and materials that are too reflective at the laser wavelength may need some sort of coating that absorbs the energy. Because of this, iteration is necessary to determine the amount of energy needed to transfer enough energy to the film without damaging it.

C. Processing

The acoustic response was recorded at a sampling frequency of 100 kHz using an electret condenser microphone located on the opposite side of the film from the excitation. The laser was externally triggered using a Digilent Analog Discovery, which also collected the microphone data via an oscilloscope channel and provided the voltage for the microphone. For each of the data sets shown here, many tests were averaged together to increase the signal-to-noise ratio. The battery film spectra are the result of 1000 tests for each film, while the drying results are each an average of 200 tests. The Fast Fourier Transform (FFT) of these averaged data was computed to find the frequency response, and from this, the power spectral density was calculated.

IV. RESULTS

A. Battery films

The averaged microphone measurements (from 1000 tests) of three different cathodes and a noise reading are shown in Fig. 9. The acoustic spectra computed from these

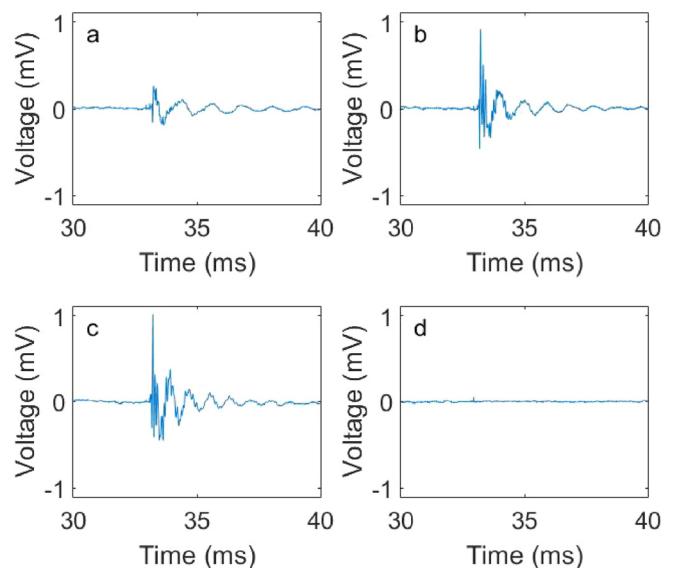


FIG. 9. Time-domain measurements for various battery films clamped in the steel clamp as shown in Fig. 8. All of the films are cathode electrodes with different coating thicknesses on $20\text{ }\mu\text{m}$ aluminum, and all measurements are an average of 1000 tests. (a) $42\text{-}\mu\text{m}$ -thick coating, (b) $38\text{-}\mu\text{m}$ -thick coating, (c) $26\text{-}\mu\text{m}$ -thick coating, and (d) baseline reading with laser off to get room/electrical noise reading for comparison.

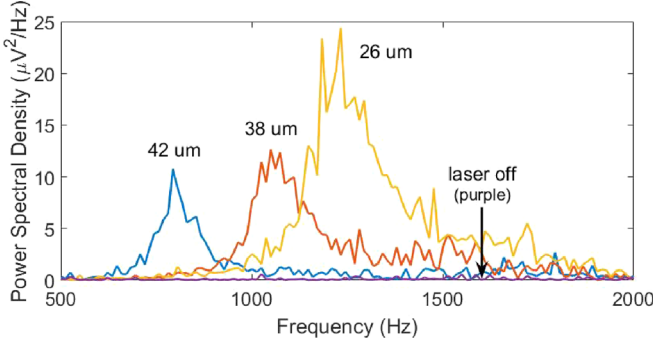


FIG. 10. Power spectral density for various battery films clamped as shown in Fig. 8. All of the films are cathode electrodes with different coating thicknesses (26 μm , 38 μm , and 42 μm) on 20 μm aluminum. The purple line labeled “laser off” is a baseline reading to ensure that the peaks seen are not due to room noise. The spectra here were obtained from the time-domain measurements shown in Fig. 9.

measurements are shown in Fig. 10. The resonances of three cathodes with a 20 μm aluminum current collector are seen to occur at different frequencies. Each of the cathodes had coating layers of different thicknesses (42 μm , 38 μm , and 26 μm coatings on top of the current collector) and densities. A baseline reading [Fig. 9(d)] was taken with the laser beam off to determine what frequencies, if any, are caused by external noise in the room. This baseline is also included in Fig. 10 to demonstrate that the peaks shown are not due to room noise.

B. Drying tests

We also found that the resonance frequency changes with other factors, such as drying. This was tested by putting a 28.0 g drop of acrylic paint (Apple Barrel brand matte acrylic paint) onto aluminum foil (about 23 μm thick) while it was in the clamp. By taking resonance tests before, after, and as the paint dried, we monitored how the resonance frequency changed over time. Without paint, the aluminum had a resonance of about 1200 Hz (shown by the dashed line in Fig. 11 and the filled circle in Fig. 12). For clarity, only results from every 20 min are shown in Fig. 11, while Fig. 12 shows where the peak occurred for all of the tests, which

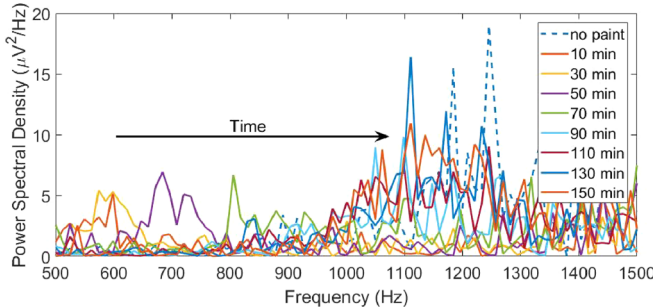


FIG. 11. The shift in frequency peaks for an aluminum film with a drying layer of paint. The peaks were identified from the acoustic response spectra of the film, clamped as shown in Fig. 8. Resonance tests were taken before paint was applied (dashed line) and every 5 min as the paint dried. In order to better distinguish peaks, only the results from tests taken every 20 min are shown in this graph. The peaks shift to higher frequencies as the paint dries, as indicated by the arrow, with the largest shift occurring between 70 and 90 min.

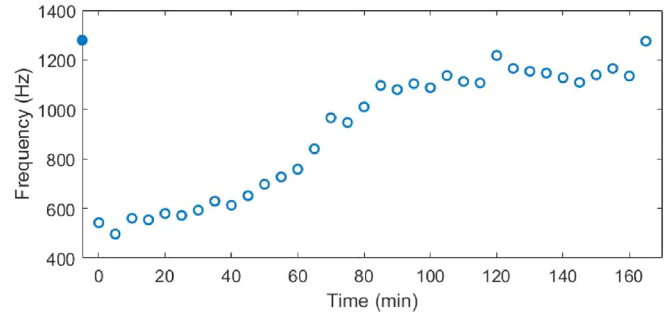


FIG. 12. The shift in frequency peaks for an aluminum film with a drying layer of paint. The peaks were identified from the acoustic response spectra of the film seen in Fig. 11. Resonance tests were taken before paint was applied (filled circle) and every 5 min as the paint dried. The peak shifts to higher frequencies as the paint dries.

were taken every 5 min. Since the results were noisy and did not always have a single clear peak, the peak values shown in Fig. 12 were found by fitting a Gaussian curve to the power spectral density obtained from the microphone data.

V. DISCUSSION

A. Thin plate/membrane behavior in results

Using the setup shown in Fig. 8 resulted in resonance tests that were able to distinguish between different commercial-grade battery films. Our experimental results appear to validate our simulations. The simulations showed that the aluminum film acted more like a plate, with h (thickness) dependence, while the battery film acted more like a membrane, with $\sqrt{1/h}$ dependence. The variation in the battery film thickness was only in the coating thickness, which has a much lower stiffness than the aluminum current collector. This likely made the effect more of a mass-loading effect, rather than having an increased stiffness.

We also found that the cathodes used in the test for Fig. 10 had coatings with different densities. The thickness and density values (calculated using the weight and reported thickness) are listed in Table II. This variation in density should also have some effect on the resonance frequency, as seen in Fig. 6, and could account for why the frequency shift seen in Fig. 10 between the coatings with a 4 μm difference is similar to the shift between those with a 12 μm thickness difference. From our analytical model in Eq. (3), we expect the thicker (and more massive) films to have a lower resonance, and this is the case with both the simulation in Fig. 5 and the experimental results in Fig. 10.

TABLE II. Measured and calculated properties of the battery films. The thickness is the reported value from the manufacturers (of the coating only, not including the 20- μm -thick aluminum current collector), the density is the calculated value, the Poisson’s ratio is assumed,²⁶ and the Young’s modulus values are obtained from a combination of simulated and experimental results (discussed below).

Coating	h (μm)	ρ (g/cm^3)	E (GPa), SLDV	E (GPa), peaks	ν
1	42	2.760	0.344	0.412	0.3
2	38	3.055	1.71	2.01	0.3
3	26	2.479	5.04	4.13	0.3

The area interrogated is quite large with respect to the microstructure of battery films and the length scales over which heterogeneities are typically measured (cm compared to μm). To further ensure that the data were representative of the entire film, four different samples were obtained from each type of film and used to excite acoustic resonances to avoid any perturbations that might be caused by significant local variation or absorption parameters. However, the resonance peaks obtained from the measurements were not always consistent, as seen from the resonance frequency averages and 95% confidence intervals listed in Table III. As mentioned previously, the values for the peaks at each location were found by fitting a Gaussian curve to the power spectral density calculated from the average of 1000 microphone measurements. The confidence intervals for some of the cathodes overlap, and the range is significant (about 200–400 Hz). Some of the natural variation could be due to deformations or non-uniformities in the battery films themselves. Systematically, the clamping may not have been completely equal all around the circumference of the film, which could also introduce additional variation in the measurements. Both natural and systematic variations need to be investigated further in future work, along with an examination of the heterogeneity of the film's properties across a larger area in order to determine how many measurements are needed to sufficiently characterize a film.

Our efforts to consistently and securely clamp the edges of the film caused a calendering effect outside of the area of interrogation. The material in the film coating was being compressed by the clamp, resulting in a change in the physical properties. Li-ion films are calendered during the manufacturing process in order to achieve a specific porosity and thickness.³⁵ This porosity affects the electronic properties of the battery and changes the density of the overall film. When we changed the porosity with our clamping, it did not change the properties of the part of the film that was currently being measured (as that was the area within the confinement), but it meant that we could not repeat measurements in the same place on our film. We are currently experimenting with other techniques for this experiment that do not calender the edges of the electrode.

The drying tests show an interesting interplay between changing mass and stiffness. When paint is first applied, it mainly acts like an added mass and decreases the resonance frequency by a large amount. As the paint dries, material evaporates, lowering the mass-loading and leading to an expected increase in frequency from the wet paint case. The paint also changes the stiffness of the composite film, further increasing the resonance. We suspect this is the reason that

TABLE III. Frequency peaks and 95% confidence intervals of the three battery films tested in the setup shown in Fig. 8. The peaks were identified by fitting a Gaussian curve to the spectra, such as those in Fig. 10.

Material	Average peak (Hz)	95% Confidence intervals (Hz)
Coating 1	848.2	731.7–964.7
Coating 2	1072	990.5–1153
Coating 3	1229	1047–1410

the resonance of the foil with fully dried paint was similar to the resonance of the foil without paint; the stiffness changed, offsetting the decrease in frequency due to the final amount of additional mass. The wet drop weighed 28.0 g, but the dry paint weighed only 9.7 g, so a significant amount of mass was lost as the paint dried. The analytical model for thin plates given by Eq. (1), which predicts the behavior of aluminum films quite well, also predicts that additional mass or density will cause the resonance frequency to decrease. However, this particular system with the paint cannot be represented well by the simplified model. Since the drop of paint nearly covered the vibration area of the film, the painted aluminum becomes almost a two-layer system, which the simulations show is not approximated well by the thin plate model. There are several other complicating factors, such as varying thickness of the paint layer across the drop, an unknown volume change from the wet drop to dry, and an unknown change in stiffness.

Drying tests such as these could have applications for the battery manufacturing process, as it shows that the acoustic response changes as the film dries. This could allow for monitoring of the drying state of the electrode during the drying of the slurry that forms the coating on the current collector.³⁵

B. Extracting Young's modulus

One interesting aspect of our acoustic measurement method is the potential to extract the Young's modulus of the battery coating. By fitting the acoustic measurements to the results of the numerical model, the Young's modulus could be found.

To ensure that the peaks we obtained from our measurements were indeed the fundamental frequencies of each film, we used a scanning laser Doppler vibrometer (SLDV) to examine the clamped cathodes. For the SLDV measurements, the films were excited with a large speaker playing a frequency chirp from 100 Hz to 5 kHz and the resulting velocity of the films was measured using a Polytec PSV-400 scanning vibrometer. For each film, we had 60–100 locations for the laser and took an average of 5 chirps to obtain the data for each location. The velocity maps obtained from the SLDV results confirmed that the peaks in Fig. 10 are the fundamental frequencies (mode 1 as seen in Fig. 3) of the three cathodes. For the film with a 42- μm -thick coating, the chirp also excited the second symmetric mode (mode 6 as seen in Fig. 3), giving two data points to fit with the simulation results.

In Fig. 13, we have the simulated results for the first four unique resonance frequencies for a film with the density and thickness for “Coating 1” listed in Table II, along with the peak values for modes 1 and 6 obtained from the SLDV results for that film (shown by the dashed lines). We ran simulations with a wide variety of values for the Young's modulus to fit the measured resonances to the data to find the elasticity of our film. The Young's modulus value given by mode 1 is 344 MPa, and the value given by mode 6 is 87.3 MPa. This difference could be caused by inaccuracy in the numerical model. It could also be due to the relatively

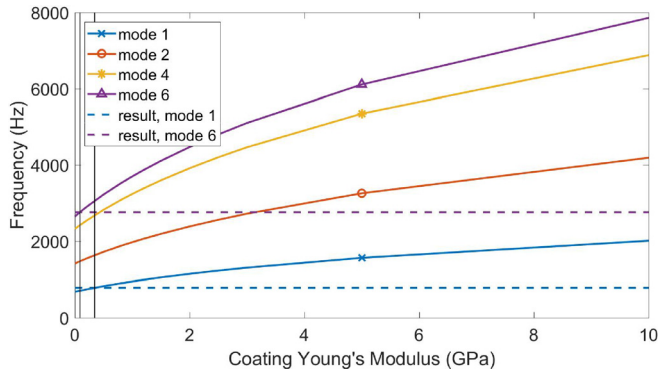


FIG. 13. Simulation of the battery cathode with properties listed under “Coating 1” in Table II. For the simulation, the Young’s modulus of the coating was varied to find the resonance frequencies. The dashed lines show the frequencies of the peaks for this film in our experimental results with the SLDV (modes 1 and 6), and the vertical lines show where the intersections occur between the simulation modes 1 and 6 and the SLDV results.

low resolution of the SLDV results. Increasing the number of averages or the number of scan points for the SLDV scan may have resulted in a slightly different frequency peak.

The result obtained using mode 1 is likely more trustworthy for several reasons. The shift in frequency caused by changing the mesh size is smaller for the lower modes than for the higher ones, so the lower frequency is less sensitive to the simulation mesh size, even though the slope for the lower mode (as seen in Fig. 13) makes the extracted Young’s modulus more sensitive to frequency changes than the higher mode. Furthermore, there is less energy in the higher modes, since the first mode is preferentially excited.³⁶ This is seen in the frequency content for the films, where the first mode has the largest peak. Additionally, at higher frequencies, such as those correlated with mode 6, the wavelength of the frequency is closer to the size of the particles in the coating through which the vibration is traveling. This means that there is more scattering of the higher frequency waves, making them less reliable. More complicated mode shapes, such as those associated with higher frequencies, have more nodes and therefore require more perfect interaction between waves to create the standing wave pattern for that shape.

Figures 14 and 15 show the simulated and SLDV results for the cathodes with coating thicknesses of 38 μm and 26 μm , respectively. Table II lists the values obtained for the Young’s modulus of each cathode from comparing the simulations with the peaks from the SLDV results (E , SLDV), as well as the values from comparing the simulations and the peaks seen in Fig. 10 (E, peaks). The peaks for each method, though similar, were not exactly the same, resulting in some difference in the extracted Young’s modulus for each film. This could be due to heterogeneity in the cathodes or the different excitation methods. A higher resolution for the FFT in the SLDV measurements, as well as narrower bandwidth frequency chirps, would also give more accurate results which may correlate better with the other tests.

The Young’s modulus values obtained from the combination of SLDV results and the numerical model are higher than most of the values seen in the literature, which range from MPa to GPa. Forouzan *et al.* measured the elasticity of

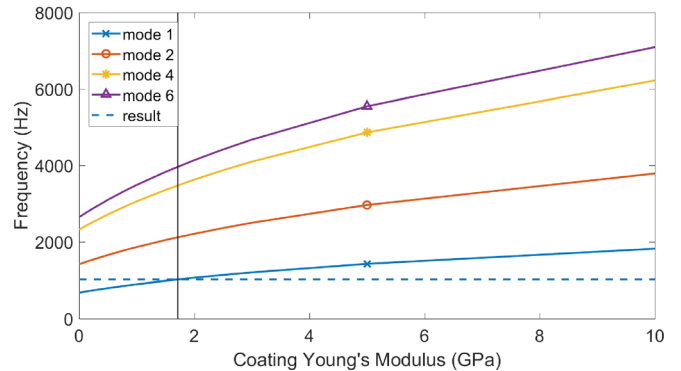


FIG. 14. Simulation of the battery cathode with properties listed under “Coating 2” in Table II. For the simulation, the Young’s modulus of the coating was varied to find the resonance frequencies. The dashed line shows the frequency of the peak for this film in our experimental results with the SLDV, and the vertical line shows the intersection between mode 1 of the simulation results and the SLDV result.

the coating (once delaminated from the current collector) and found it to be about 11.3 MPa,³² while Nadimpalli *et al.* used the rule of mixtures to calculate a cathode coating elasticity of 40 GPa.³⁷ The rule of mixtures does not account for how materials actually interact, so the measured value is likely more reliable, but much lower than those obtained from our experiments. However, with such a large range for the elasticity of the battery coating, it is difficult to have a good benchmark for the Young’s modulus values shown here.

VI. CONCLUSION

Battery safety and quality could be improved by reducing heterogeneities in battery electrode films. Measuring acoustic resonances of these films and looking for shifts in the resonance is one way to monitor changes in the mechanical properties. We were able to use a laser to excite resonances in commercial battery cathodes and distinguish between films with different coating thicknesses, as our simulations predicted would be possible. Acoustic response could also be used to monitor the state of drying, as we were able to detect

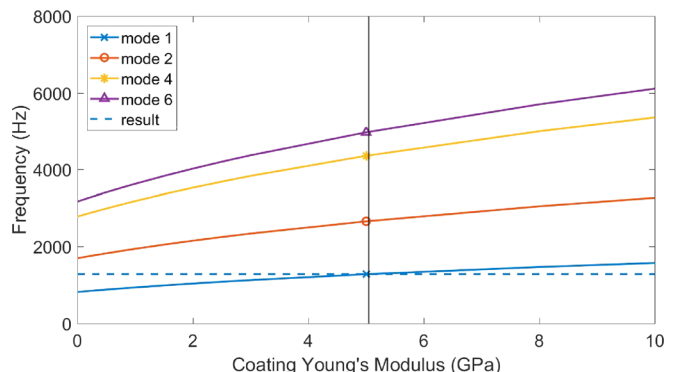


FIG. 15. Simulation of the battery cathode with properties listed under “Coating 3” in Table II. For the simulation, the Young’s modulus of the coating was varied to find the resonance frequencies. The dashed line shows the frequency of the peak for this film in our experimental results with the SLDV, and the vertical line shows the intersection between mode 1 of the simulation results and the SLDV result.

changes in mass and stiffness during a drying process. Additionally, the combination of resonance measurements and a numerical model can enable the determination of the Young's modulus of the battery film, which is difficult to measure. Although more work is needed in this area, acoustic resonance measurements could be a form of fast, non-destructive quality control in battery manufacturing.

ACKNOWLEDGMENTS

This work was supported by the U.S. Department of Energy through the BMR program. K.D. also acknowledges support from the Utah NASA Space Grant Consortium Fellowship. We gratefully acknowledge the assistance of Brian Anderson and Sarah Young to perform the SLDV measurements.

- ¹G. Chen and T. Richardson, *J. Power Sources* **195**, 5387 (2010).
- ²S. J. Harris and P. Lu, *J. Phys. Chem. C* **117**, 6481 (2013).
- ³B. J. Lanterman, A. A. Riet, N. S. Gates, J. D. Flygare, A. D. Cutler, J. E. Vogel, D. R. Wheeler, and B. A. Mazzeo, *J. Electrochem. Soc.* **162**, A2145 (2015).
- ⁴K. Zeng and J. Zhu, *Mech. Mater.* **91**, 323 (2015).
- ⁵G. Chow, P. Miller, and J. Wang, *Exp. Mech.* **55**, 647 (2015).
- ⁶S. S. Kumar, A. Fartash, M. Grimsditch, I. K. Schuller, and R. S. Kumar, *Macromolecules* **26**, 6184 (1993).
- ⁷A. G. Every, *Meas. Sci. Technol.* **13**, R21 (2002).
- ⁸D. Schneider and M. Tucker, *Thin Solid Films* **290**, 305 (1996).
- ⁹A. Neubrand and P. Hess, *J. Appl. Phys.* **71**, 227 (1992).
- ¹⁰D. Hurley, V. Tewary, and A. Richards, *Thin Solid Films* **398**, 326 (2001).
- ¹¹R. Côte, T. V. der Donck, J.-P. Celis, and C. Glorieux, *Thin Solid Films* **517**, 2697 (2009).
- ¹²T. Grabec, P. Sedlák, P. Stoklasová, M. Thomasová, D. Shilo, M. Kabla, H. Seiner, and M. Landa, *Smart Mater. Struct.* **25**, 127002 (2016).
- ¹³G. Chow, E. Uchaker, G. Cao, and J. Wang, *Mech. Mater.* **91**(Part 2), 333 (2015).
- ¹⁴J. Sermeus, R. Sinha, K. Vanstreels, P. M. Vereecken, and C. Glorieux, *J. Appl. Phys.* **116**, 023503 (2014).
- ¹⁵S. Kitazawa, A. Chiba, and E. Wakai, *Nucl. Instrum. Methods Phys. Res., Sect. A* **786**, 47 (2015).
- ¹⁶Q. Zhang, X. Xiao, Y.-T. Cheng, and M. W. Verbrugge, *Appl. Phys. Lett.* **105**, 061901 (2014).
- ¹⁷S. E. Bobbin, J. W. Wagner, and R. C. Cammarata, *Appl. Phys. Lett.* **59**, 1544 (1991).
- ¹⁸W. Gao, C. Glorieux, and J. Thoen, *Int. J. Eng. Sci.* **41**, 219 (2003).
- ¹⁹C. Prada, O. Balogun, and T. W. Murray, *Appl. Phys. Lett.* **87**, 194109 (2005).
- ²⁰C. M. Grünsteidl, I. A. Veres, and T. W. Murray, *J. Acoust. Soc. Am.* **138**, 242 (2015).
- ²¹A. G. Hsieh, S. Bhadra, B. J. Hertzberg, P. J. Gjeltema, A. Goy, J. W. Fleischer, and D. A. Steingart, *Energy Environ. Sci.* **8**, 1569 (2015).
- ²²A. Fartash, *Appl. Phys. Lett.* **61**, 2024 (1992).
- ²³A. Biswas, T. Weller, and L. P. B. Katehi, *Rev. Sci. Instrum.* **67**, 1965 (1996).
- ²⁴C. Malhaire, *Rev. Sci. Instrum.* **83**, 055008 (2012).
- ²⁵F. Gamboa, A. López, F. Avilés, J. E. Corona, and A. I. Oliva, *Meas. Sci. Technol.* **27**, 045002 (2016).
- ²⁶L. Kinsler, A. Frey, A. Coppens, and J. Sanders, *Fundamentals of Acoustics*, 4th ed. (Wiley-VCH, New York, 1999).
- ²⁷S. Timoshenko, D. H. Young, and W. Weaver, Jr., *Vibration Problems in Engineering*, 4th ed. (John Wiley & Sons, Inc., New York, 1974).
- ²⁸E. Ruggiero, Ph.D. dissertation, Virginia Polytechnic Institute and State University, Blacksburg, VA, 2005.
- ²⁹A. Fartash, I. K. Schuller, and M. Grimsditch, *J. Appl. Phys.* **71**, 4244 (1992).
- ³⁰N. H. Fletcher, *Acoustic Systems in Biology* (Oxford University Press, New York, 1992).
- ³¹L. Dong, M. Grissom, and F. T. Fisher, *AIMS Energy* **3**, 344 (2015).
- ³²M. M. Forouzan, C.-W. Chao, D. Bustamante, B. A. Mazzeo, and D. R. Wheeler, *J. Power Sources* **312**, 172 (2016).
- ³³B. Liu, X. Feng, and S.-M. Zhang, *Compos. Sci. Technol.* **69**, 2198 (2009).
- ³⁴J. Hatch, *Aluminum: Properties and Physical Metallurgy* (ASM International, Metals Park, OH, USA, 1984), Chap. 1, pp. 13–14.
- ³⁵K. Tagawa and R. Brodd, in *Lithium-Ion Batteries: Science and Technologies*, edited by M. Yoshio, R. Brodd, and A. Kozawa (Springer, New York, NY, USA, 2009), Chap. 8, pp. 181–194.
- ³⁶R. D. Costley, M. E. Henderson, H. Patel, E. W. Jones, G. M. Boudreux, and M. J. Plodinec, *NDT&E Int.* **40**, 300 (2007).
- ³⁷S. P. Nadimpalli, V. A. Sethuraman, D. P. Abraham, A. F. Bower, and P. R. Guduru, *J. Electrochem. Soc.* **162**, A2656 (2015).